Available online at www.sciencedirect.com
SCIENCE DIRECT
Journal of Catalysis 235 (2005) 378–392
JOURNAL OF CATALYSIS
www.elsevier.com/locate/jcat

Distinguishing between reaction intermediates and spectators: A kinetic study of acetone oxidation using ozone on a silica-supported manganese oxide catalyst

Corey Reed [a], Yan Xi [a], S. Ted Oyama [a,b,*]

[a] *Environmental Catalysis and Nanomaterials Laboratory, Department of Chemical Engineering, Virginia Polytechnic Institute and State University, Blacksburg, VA 24061-0211, USA*

[b] *Department of Chemistry, Virginia Polytechnic Institute and State University, Blacksburg, VA 24061-0211, USA*

Received 7 June 2005; revised 20 August 2005; accepted 23 August 2005

Abstract

A detailed mechanistic study of acetone oxidation using ozone was performed on a 10 wt% silica-supported manganese oxide catalyst using in situ Raman spectroscopy. Two adsorbed intermediates were identified at reaction conditions: an acetone species with a band at 2930 cm^{-1} and an adsorbed peroxide species on the manganese oxide with a band at 890 cm^{-1}. Quantitative temperature-programmed desorption measurements showed that the acetone species resided on the silica support, which thus acted as a noninnocent support. The rates of the acetone and ozone reactions at 318–373 K were equally well described by the power-rate law and Langmuir–Hinshelwood expressions. Transient experiments showed that the rates of formation and reaction of the peroxide surface species did not correspond to the overall reaction rate, and it was concluded that it was not directly involved in the main reaction pathway. A mechanism is proposed involving the migration of the adsorbed acetone intermediate from the silica support to manganese centers, where it reacts with atomically adsorbed oxygen species to form complete oxidation products.

Keywords: Acetone; Ozone; Catalytic oxidation; Kinetics; Mechanism; Transient methods; Raman spectroscopy; Spectator

1. Introduction

Monitoring adsorbed intermediates on catalyst surfaces during reaction conditions is an effective means of elucidating mechanistic information for catalytic reactions [1]. However, proof that the observed surface species are true reaction intermediates has been provided only infrequently. Such proof would include measurement of the rates of formation and consumption of the intermediates and confirmation that these rates were consistent with the overall reaction rate. This study provides such a quantitative comparison for acetone oxidation with ozone on manganese oxide. Manganese oxide was chosen for study because it is one of the most active transition metal oxides for total oxidation. This topic is relevant to air pollution control for the removal of volatile organic compounds (VOCs). Although catalytic oxidation is effective in removing high concentrations of VOCs from large-volume gas emissions, it generally requires temperatures above 873 K [2]. The use of ozone allows complete removal of VOCs at close to room temperature, resulting in an estimated 1.5 times greater energy savings compared with conventional catalytic incineration [3].

In previous work [4], the reactivity of 3 and 10 wt% silica-supported manganese oxide catalysts for the oxidation of acetone was found to be enhanced by ozone compared with oxygen, resulting in a dramatic decrease in activation energy. The activity of the 10 wt% MnO_x/SiO_2 catalyst proved to be greater than that of the 3 wt% MnO_x/SiO_2 catalyst because of structural differences in the two catalysts [4]. Further work [5] using in situ Raman spectroscopy on the 10 wt% MnO_x/SiO_2 catalyst identified an adsorbed acetone intermediate with a vibrational band at 2930 cm^{-1} and a peroxide species formed from ozone with a characteristic band at 890 cm^{-1}. Both intermediates were observed simultaneously during reaction conditions [5]. The

* Corresponding author.
E-mail address: oyama@vt.edu (S.T. Oyama).

0021-9517/$ – see front matter
doi:10.1016/j.jcat.2005.08.014

present study looks at the role of the intermediates and also examines the kinetics of the oxidation of acetone using ozone over the 10 wt% MnO_x/SiO_2 catalyst. The study includes both steady-state and transient kinetic analysis and uses in situ Raman spectroscopy to measure surface coverage. Two kinetic models are discussed, and a reaction mechanism is proposed.

Many techniques have been used to study surface intermediates. Notable among these are vibrational spectroscopy techniques, such as sum frequency generation (SFG), Fourier transform infrared spectroscopy (FTIR), and Raman spectroscopy, which provide direct molecular information. SFG has indicated that the hydrogenation of cyclohexene to cyclohexane on Pt(111) at 300–400 K involved a reactive 1,3-cyclohexadiene intermediate [6]. SFG also has shown that the hydrogenation of ethylene on Pt(111) occurred mainly through a π-bonded ethylene species [7].

In situ FTIR studies of methanol oxidation over a MoO_3/SiO_2 catalyst showed that the methanol formed mobile methoxide species on the silica support that migrated and reacted to form formaldehyde on the Mo centers [8,9]. The silica support displayed noninnocent behavior [9], actively participating in the reaction by holding reactive intermediates. FTIR also showed that in the reaction of CO and H_2 to form CH_4 on a Rh/Al_2O_3 catalyst at 220 K, there were small concentrations of surface carbon species, CH_x, large amounts of adsorbed CO species, and spectator C_xH_y species [10]. Another IR study showed that the decomposition of methanol over Cu/SiO_2 involved adsorbed methoxide species that dehydrogenated to form formaldehyde and formate species and then decomposed to CO_2 and H_2 [11]. Finally, an in situ IR study found that the hydroformylation of ethylene to propionaldehyde over $Mn–Rh/SiO_2$ involved acyl C_2H_5CO intermediates [12]. Raman spectroscopy indicated that in the decomposition of nitrous oxide over a BaO on MgO (Ba/MgO) catalyst peroxide ions served as both an intermediate and a poison in the reaction [13].

Previous studies have provided examples in which adsorbed intermediates were identified during reaction conditions to help provide mechanistic information for catalytic reactions. The present work focuses on the oxidation of acetone using ozone. As we show, adsorbed surface species observed by Raman spectroscopy respond to reaction conditions in a manner resembling the reaction intermediates. However, transient experiments show that these species do no respond at rates consistent with the overall reaction rate and thus are not the principal reactive intermediates. This work is important because it highlights the need for dynamic experiments to prove that spectroscopically observed species are involved in a mechanism.

To our knowledge, the mechanism and kinetics of the oxidation of acetone by ozone over a manganese oxide catalyst has not yet been studied. Previous work [14,15] investigated the kinetics and mechanism for ozone decomposition over manganese oxide, as discussed later in this paper. An understanding of this mechanism is important for the present study, because ozone decomposition proceeds simultaneously with acetone oxidation. The kinetics for the ozone decomposition reaction used steady-state measurements that were confirmed by transient measurements [15]. This technique, which will be called the Tamaru method after its originator, was first used to derive kinetic information for the ammonia decomposition reaction on tungsten [16].

2. Experimental

2.1. Materials

A 10 wt% manganese oxide catalyst (using MnO_2 as the basis) was used for all experiments. The synthesis details are reported elsewhere [4], but briefly, the catalyst was prepared by incipient wetness impregnation of an aqueous solution of manganese acetate ($Mn(CH_3COO)_2 \cdot 4H_2O$, 99.9%; Aldrich) on a SiO_2 support, followed by drying and calcination at 773 K.

The gases used in this study included oxygen (>99.6%; Air Products) and helium (>99.6%; Air Products), which were passed through gas purifiers (Alltech, model 4658) to eliminate moisture. Acetone (99.9+%; Burdick and Jackson) was used as received.

2.2. Spectroscopic and kinetic measurements

Laser Raman spectroscopy and kinetic data were obtained using a combined reactor system (Fig. 1) as described previously [5]. Briefly, the spectroscopic part of the system comprised an argon ion laser (514.5 nm; Spex Lexel 95), a holographic notch filter (Kaiser; Super Notch Plus), a single-stage monochromator (Spex; 500 M), and a CCD detector (Spex; Spectrum One). The powder catalyst sample (~0.2 g) was pressed (201 MPa) into a thin wafer (1.5 cm diameter, 0.1 cm thick) and was held in place by a stainless steel cap at the end of a rotating ceramic rod. The sample was enclosed by a synthetic quartz (Suprasil) cell provided with inlet and outlet ports to serve as an in situ reactor. The cell was wrapped in heating tape, and a thermocouple was placed in a well just 0.3 cm away from the catalyst sample to measure the temperature. The gas delivery part of the system included a two-stage bubbler used for the vaporization of liquid acetone. The Antoine equation [17] was used to obtain the acetone vapor pressure (9.25 kPa at 273 K), and the flow rate of helium (6.8 μmol/s ≈ 10 cm^3/min) was adjusted to give the desired gas-phase acetone concentration. Pure oxygen (120 μmol/s = 180 cm^3/min) was fed to an ozone generator (OREC; V5-0), which produced ozone through corona discharge, and the exit ozone concentration was measured with an ozone monitor (In USA; model H1). A gas chromatograph (SRI; model 8610C) equipped with flame ionization and thermal conductivity detectors was used for measuring acetone, CO, and CO_2 concentrations.

Before all measurements, the catalyst sample was pretreated at 723 K for 2 h in a mixture of oxygen and helium to remove excess moisture and carbonaceous impurities from the sample. A secondary helium flow (220 μmol/s = 320 cm^3/min) was added to make the total flow rate of the feed for all experiments (340 μmol/s = 500 cm^3/min), which was composed of 35 mol% oxygen and 65 mol% helium. The concentrations of

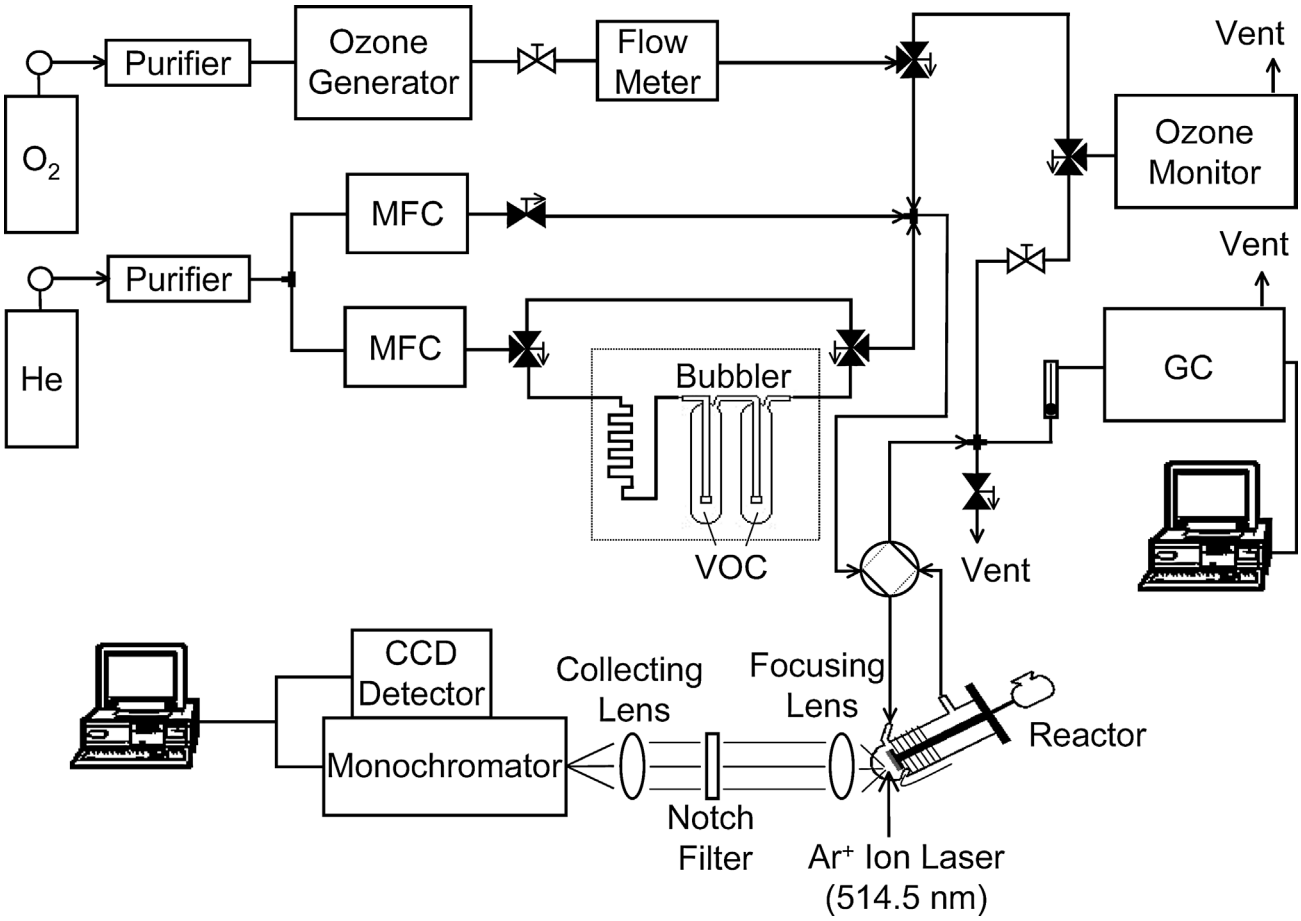

Fig. 1. In situ Laser Raman spectroscopy system.

acetone and ozone were varied for the experiments but were always $\leqslant$1.0 mol%.

Detailed kinetic measurements were performed for the oxidation reaction of acetone and ozone over the 10 wt% MnO_x/SiO_2 catalyst. In one set of experiments, the inlet partial pressure of acetone was varied over the range of 101 Pa (1000 ppm) to 405 Pa (4000 ppm), whereas the inlet partial pressure of ozone was held constant at ∼790 Pa (∼7800 ppm). In another set of experiments, the inlet partial pressure of ozone was varied over the range of 101 Pa (1000 ppm) to 1013 Pa (10,000 ppm), whereas the inlet partial pressure of acetone was held constant at ∼193 Pa (∼1900 ppm). These measurements were carried out at reaction temperatures of 318, 333, 353, and 373 K while monitoring both acetone and ozone consumption rates. Similarly, blank kinetic experiments were also conducted for the reaction between acetone and ozone with no catalyst or support present in the reactor.

A previous Raman spectroscopy study carried out on the 10 wt% MnO_x/SiO_2 catalyst identified two adsorbed species on the surface of the catalyst during the reaction between acetone and ozone [5]. An acetone intermediate was found with a characteristic feature at 2930 cm^{-1}, and a peroxide species attributed to ozone was found with a feature at 890 cm^{-1}. In this work, steady-state Raman spectroscopy experiments were carried out on the 10 wt% MnO_x/SiO_2 catalyst sample to measure the coverage of the adsorbed intermediates associated with acetone and ozone. These experiments used the same conditions as used for the kinetic experiments on the 10 wt% catalyst sample, except that only the lowest reaction temperature of 318 K was used.

Transient Raman spectroscopy experiments were also performed on the 10 wt% catalyst sample at 318 K to measure the evolution of adsorbate coverage with respect to time. Acetone addition, acetone removal, ozone addition, and ozone removal experiments were conducted at initial acetone and ozone partial pressures of 193 and 793 Pa (1900 and 7800 ppm), respectively. In all cases the measurements began at steady-state (removal experiments) or ended at steady-state (addition experiments).

2.3. Temperature-programmed desorption measurements

Integrated peak areas from the Raman spectroscopy measurements were calibrated by quantitative analysis of temperature-programmed desorption (TPD) traces for acetone and ozone. The TPD measurements were conducted using a standard flow system equipped with a computer-interfaced mass spectrometer (Dycor/Ametek; model MA100). As for the kinetic and spectroscopic experiments, ∼0.2 g of the catalyst was first pretreated at 723 K for 2 h in oxygen (35 mol%) and helium (65 mol%) at a total flow rate of 340 μmol/s (500 cm^3/min). For the ozone TPD experiments, ozone (1013 Pa = 10,000 ppm) was introduced to the reactor for 1 h at 298, 273, and 261 K.

Table 1
Acetone and ozone surface area, molecular oxygen uptake, and TPD values for 10 wt% MnO_x/SiO_2 and pure SiO_2

Sample	SA (m^2/g)	O_2 uptake (μmol/g)	Ozone TPD (μmol/g)	Ozone TPD (μmol/m^2)	Acetone TPD (μmol/g)	Acetone TPD (μmol/m^2)
10 wt% MnO_x/SiO_2	210	49	14	0.067	550	2.6
SiO_2	320	0	0	0	790	2.5

Low temperatures were used to obtain saturation coverage on the catalyst surface. After the initial 1 h of treatment, the ozone was cut off, and helium was introduced to the sample at 68 μmol/s (100 cm^3/min). The sample was heated at 0.17 K/s (10 K/min) to 673 K while the desorption signal for O_2 ($m/e = 32$), the only desorption product, was monitored. The O_2 desorption peak was quantitated with pulses of pure oxygen from a calibrated dosing volume (19.6 μmol). For the acetone TPD experiments, acetone at a partial pressure of 811 Pa (8000 ppm) was introduced to the reactor for 1.5 h at 298, 273, and 261 K to obtain saturation adsorption. An identical procedure was used for the ozone experiment. A higher acetone partial pressure of 1216 Pa (12,000 ppm) was also used, but yielded the same results. The acetone desorption signal was calibrated with an acetone pulse (1.05 μmol). The acetone TPD experiment was repeated at 273 K using a pure, calcined (6 h in air at 773 K) silica sample.

3. Results

3.1. TPD measurements

Previous work done in our laboratory showed that ozone adsorbs on manganese oxide in the form of a peroxide species (O_2^{2-}) and then desorbs as molecular oxygen [14,15]. In the present investigation, ozone TPD experiments allowed the determination of the saturation amount of the adsorbed peroxide intermediate on the surface of the 10 wt% MnO_x/SiO_2 catalyst by measuring the desorption of molecular oxygen as a function of adsorption temperature. Similarly, acetone TPD experiments allowed determination of the saturation amount of the adsorbed acetone intermediate. For both the ozone and acetone TPD experiments, maximum adsorption was achieved at a treatment temperature of 273 K. Table 1 gives the results of the TPD measurements along with previously reported surface area and molecular oxygen chemisorption results [4]. Both the ozone and acetone TPD experiments yielded well-defined desorption peaks at ∼385 K for oxygen and ∼345 K for acetone. The amount of peroxide species (derived from ozone) adsorbed on the catalyst surface was 14 μmol/g, and the amount of acetone intermediate adsorbed on the catalyst surface was 550 μmol/g. The amount of atomic oxygen chemisorption was 98 μmol/g. Acetone TPD experiments done on the silica support yielded an adsorption amount for acetone of 790 μmol/g at a desorption temperature of ∼350 K.

3.2. Steady-state Raman spectroscopy measurements

Steady-state, in situ Raman spectroscopy experiments conducted on pure silica and the 10 wt% MnO_x/SiO_2 catalyst at 298 K are shown in Fig. 2. The feature at 280 cm^{-1} due to a Si–O vibration was used as an internal standard, so that a reasonable comparison could be made between different experiments on the 10 wt% MnO_x/SiO_2 catalyst, as well as measurements on pure silica. Fig. 2a displays the Raman spectrum for the 10 wt% MnO_x/SiO_2 catalyst when acetone was included in the gas mixture at a concentration of 0.2 mol%, and Fig. 2b shows the spectrum when the concentration was doubled to 0.4 mol%. The increase in acetone concentration led to a slight increase in peak intensity and area of the band attributed to the adsorbed acetone intermediate (2930 cm^{-1}). Fig. 2c shows a Raman spectrum for pure silica with acetone at a concentration of 0.2 mol%, and Fig. 2d shows the spectrum when the concentration of acetone was doubled to 0.4 mol%. Again, the increase in acetone concentration lead to an increase in peak intensity and area for the Raman band associated with the adsorbed acetone intermediate (2930 cm^{-1}). Overall the intensities were much higher on the SiO_2 than on the catalyst.

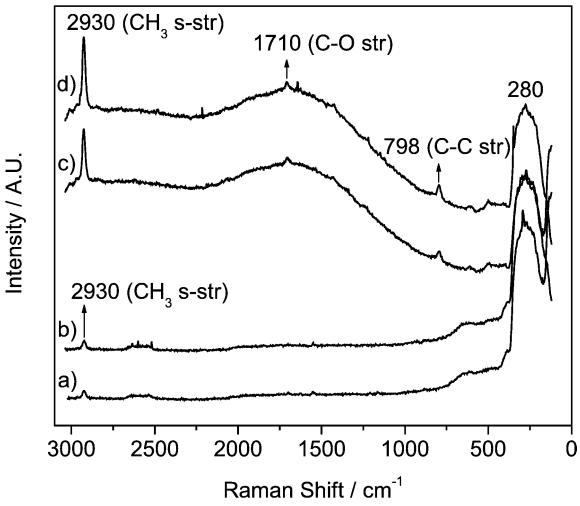

Fig. 2. Steady-state, in situ Raman spectroscopy results for pure SiO_2 and the 10 wt% MnO_x/SiO_2 sample in acetone flow at 298 K.

Steady-state, in situ Raman spectroscopy experiments were also conducted on the 10 wt% MnO_x/SiO_2 catalyst at 318 K using the same varying partial pressure conditions as used in the kinetic experiments. Fig. 3 shows the Raman spectra when the initial acetone partial pressure was varied (93–394 Pa) and the initial ozone partial pressure was kept constant (790 Pa). Fig. 4 shows the Raman spectra when the initial ozone partial pressure was varied (274–1097 Pa) and the initial acetone partial pressure remained constant (193 Pa).

Using the Raman spectra presented in Figs. 3 and 4, surface coverage values were calculated at 318 K for the two adsorbed intermediates at the different reactant partial pressure condi-

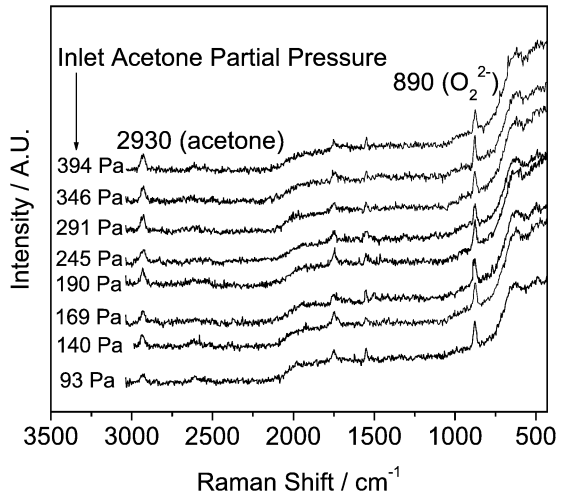

Fig. 3. Steady-state Raman spectra taken at 318 K with varying acetone partial pressure and constant ozone partial pressure at 790 Pa.

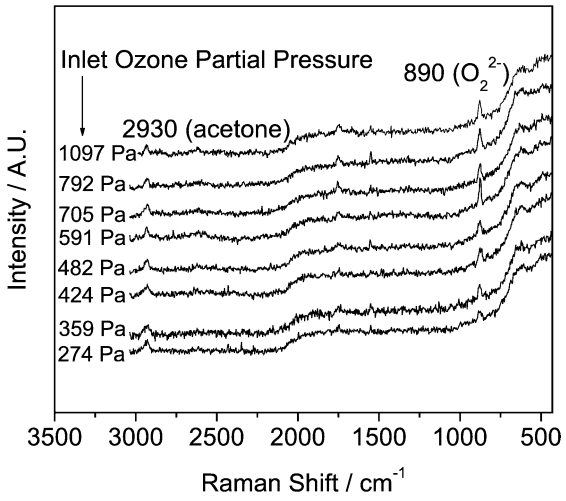

Fig. 4. Steady-state Raman spectra taken at 318 K with varying ozone partial pressure and constant acetone partial pressure at 193 Pa.

tions. The surface coverage for the acetone intermediate, θ_A, was calculated by integrating the Raman peak at 2930 cm^{-1} and dividing the resulting peak area by the area obtained when acetone alone was saturated on the surface of the catalyst. Likewise, the surface coverage for the peroxide intermediate, θ_{O_2*}, was determined by integrating the Raman peak at 890 cm^{-1} and dividing that peak area by the area obtained when the peroxide species was saturated on the catalyst surface. The saturated surface concentration of acetone (~811 Pa, 273 K) was 2.6 μmol/m^2, whereas the saturated surface concentration of the peroxide species (~1013 Pa, 273 K) was 0.067 μmol/m^2 (Table 1).

Fig. 5 shows the coverage values associated with acetone (θ_A) and ozone (θ_{O_2*}) when the initial acetone partial pressure was varied and the initial ozone partial pressure was kept constant (790 Pa). Fig. 6 shows the coverages associated with acetone (θ_A) and ozone (θ_{O_2*}) when the initial ozone partial pressure was varied and the initial acetone partial pressure was kept constant (193 Pa).

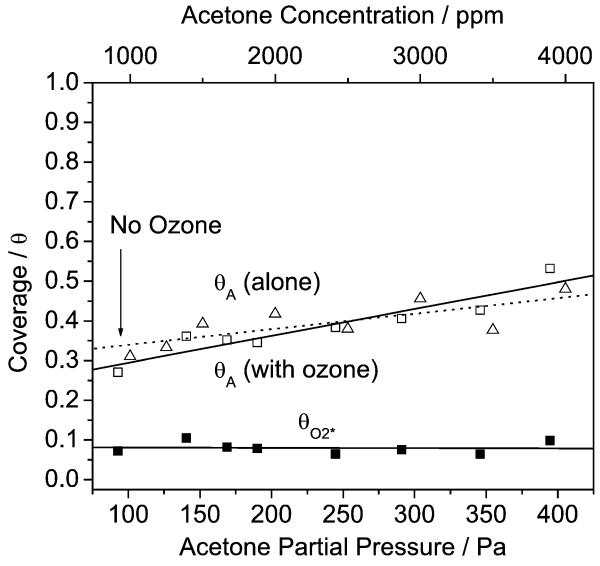

Fig. 5. Steady-state surface coverage values at 318 K for adsorbed acetone and ozone intermediates with varying acetone partial pressure is varied and constant ozone partial pressure at 790 Pa.

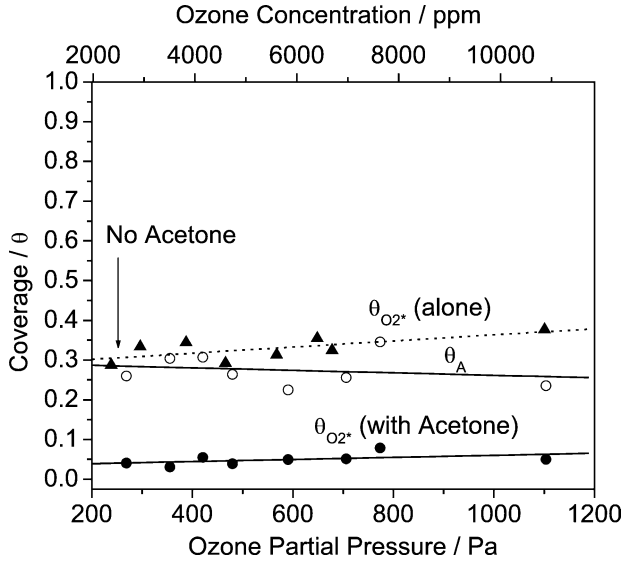

Fig. 6. Steady-state surface coverage values at 318 K for adsorbed acetone and ozone intermediates with varying ozone partial pressure and constant acetone partial pressure at 193 Pa.

3.3. Steady-state kinetic measurements

Kinetic experiments were performed to determine the rates of acetone and ozone reaction on the 10 wt% MnO_x/SiO_2 catalyst sample. The data were obtained by varying the partial pressure of one of the reactants (acetone or ozone) over a range while maintaining partial pressure of the other reactant close to the middle of the range. A blank kinetic experiment was conducted to determine the gas phase contributions to the oxidation reaction. The gas phase conversions for both acetone and ozone were subtracted from those obtained from the experiments run with catalyst, so that the calculated kinetic parameters accounted only for the reaction on the catalyst surface. The

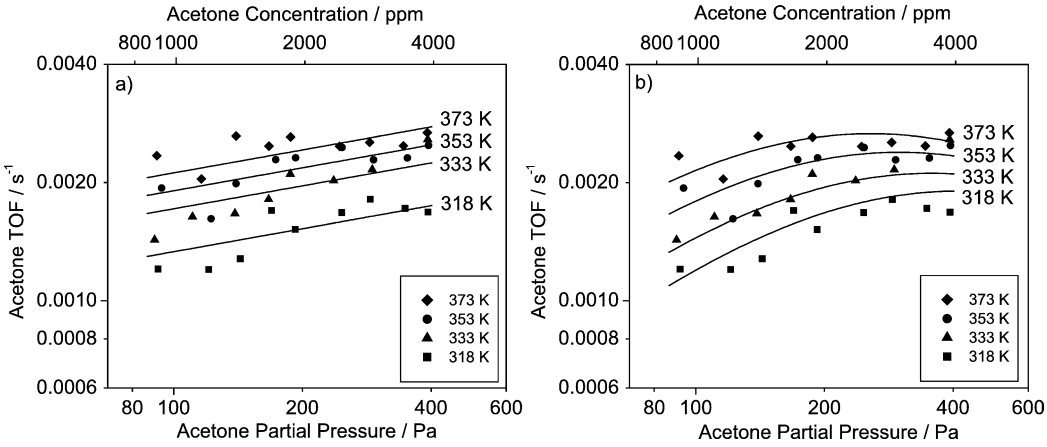

Fig. 7. Steady-state kinetic data for acetone TOF as a function of acetone partial pressure with constant partial pressure of ozone at ∼790 Pa for the (a) power-law expression and (b) Langmuir–Hinshelwood expression.

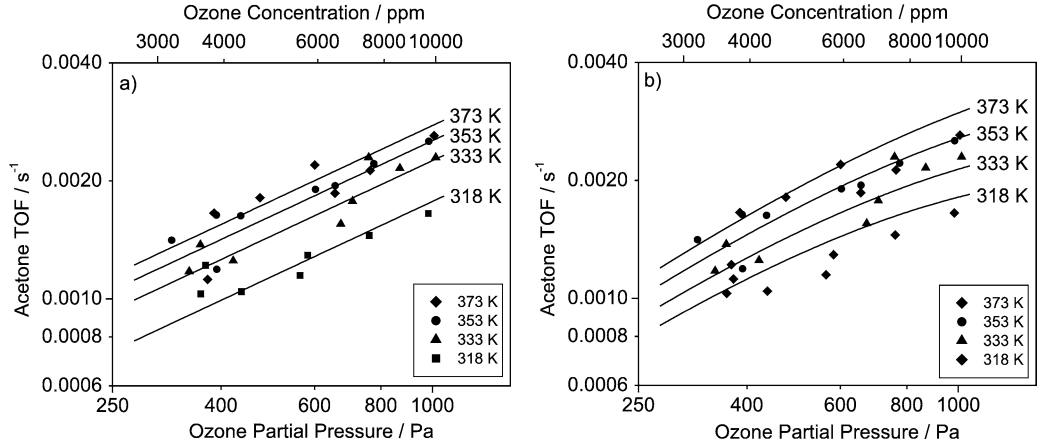

Fig. 8. Steady-state kinetic data for acetone TOF as a function of ozone partial pressure with constant partial pressure of acetone at 193 Pa (a) power-law expression and (b) Langmuir–Hinshelwood expression.

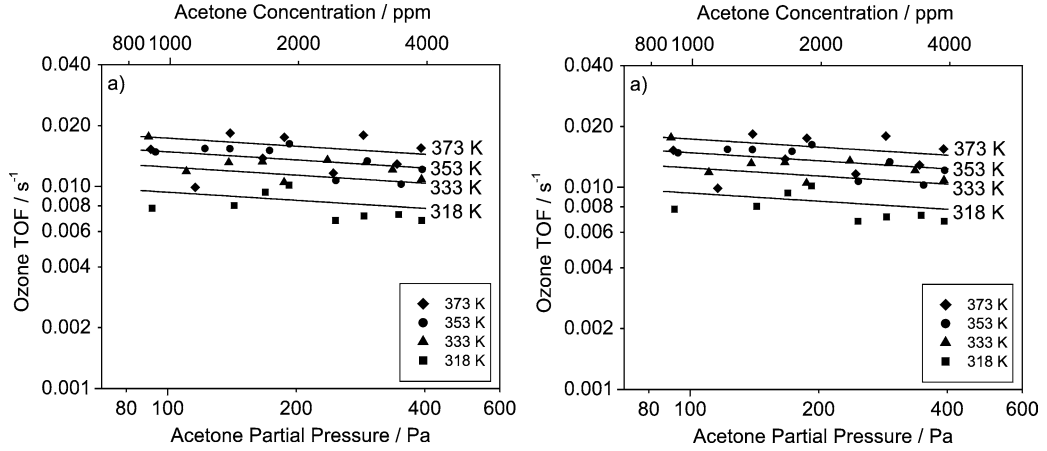

Fig. 9. Steady-state kinetic data for ozone TOF as a function of acetone partial pressure with constant partial pressure at 790 Pa (a) power-law expression and (b) Langmuir–Hinshelwood expression.

only observed product for the oxidation of acetone using ozone in the temperature range studied (333–373 K) was CO_2.

Using the conversions obtained for each reactant species, turnover frequencies (TOFs) for both acetone and ozone conversion were calculated based on the atomic oxygen uptake value (98 μmol/g) for the 10 wt% MnO_x/SiO_2 catalyst sample. Figs. 7–10 show the temperature and pressure dependencies of the acetone and ozone TOFs presented as logarithmic plots. In Figs. 7a–10a, the straight lines represent overall fits for a power-law rate expression for both acetone and ozone

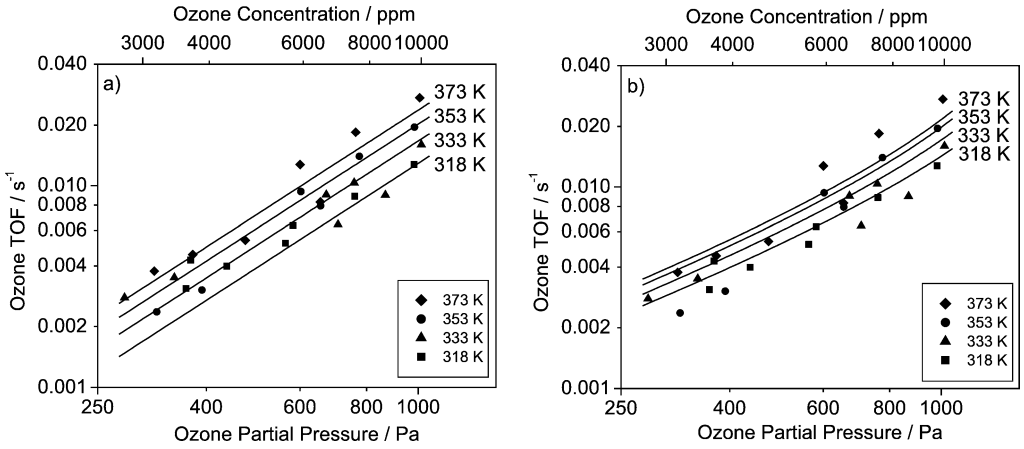

Fig. 10. Steady-state kinetic data for ozone TOF as a function of ozone partial pressure with constant partial pressure of acetone at 193 Pa (a) power-law expression and (b) Langmuir–Hinshelwood expression.

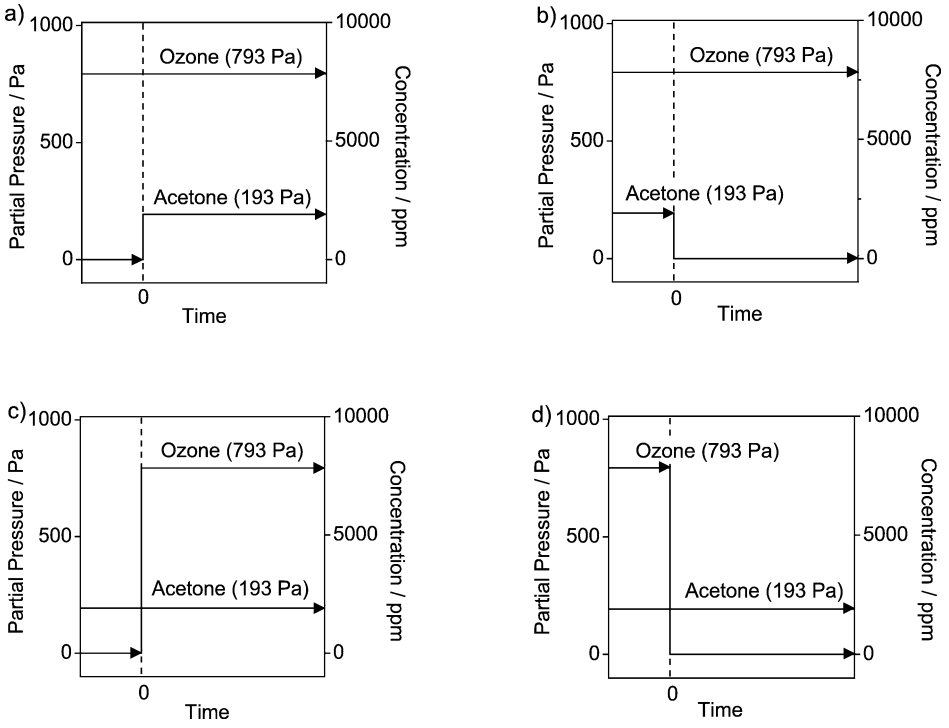

Fig. 11. Schematic depictions of transient experiments (a) acetone addition, (b) acetone removal, (c) ozone addition, and (d) ozone removal.

TOF. For Figs. 7b–10b, the curves represent fits for a derived Langmuir–Hinshelwood rate expression for both acetone and ozone TOF. The power rate law expressions were obtained by taking the concentration (mol/m^3), TOF (s^{-1}), and temperature (K) data and simultaneously fitting the entire dataset by nonlinear least squares regression analysis using the POLYMATH 5.1 program [18] to obtain the kinetic parameters; we discuss this in more detail later in the paper. The Langmuir–Hinshelwood rate expressions were obtained by taking the concentration (mol/m^3), TOF (s^{-1}), and temperature (K) data for a single temperature and fitting each dataset by nonlinear least squares regression analysis using the same program. The development of the Langmuir–Hinshelwood kinetic expression, as well as a statistical comparison of the degree of fit for the two different rate expression forms, are also discussed later.

3.4. Transient kinetic measurements

Transient, in situ Raman spectroscopy experiments were conducted on the 10 wt% MnO_x/SiO_2 catalyst at 318 K using initial partial pressures for acetone and ozone of 193 and 793 Pa (1900 and 7800 ppm), respectively. Schematic depictions of these experiments are shown in Fig. 11. Transient experiments were used so that the adsorption rate for each adsorbed intermediate could be studied separately from the rates of reaction and desorption. Fig. 12 presents the acetone addition results and includes an inset describing the inlet partial pressure profiles for the experiment. As soon as acetone was introduced, the coverage associated with the peroxide species quickly dropped to a stable value of 0.08 in ∼600 s, whereas the coverage associated with the acetone intermediate increased to a steady value

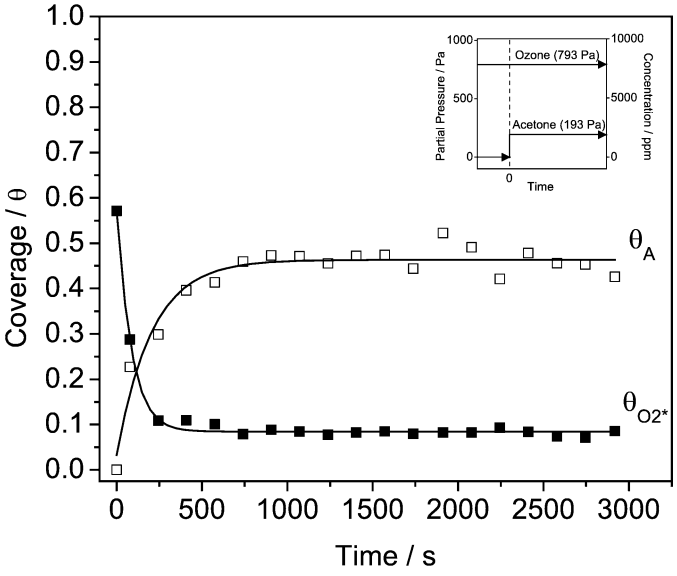

Fig. 12. Transient acetone addition results at 318 K showing coverage values for adsorbed acetone and ozone intermediates as a function of time. The inset shows the inlet partial pressure profiles used for the experiment.

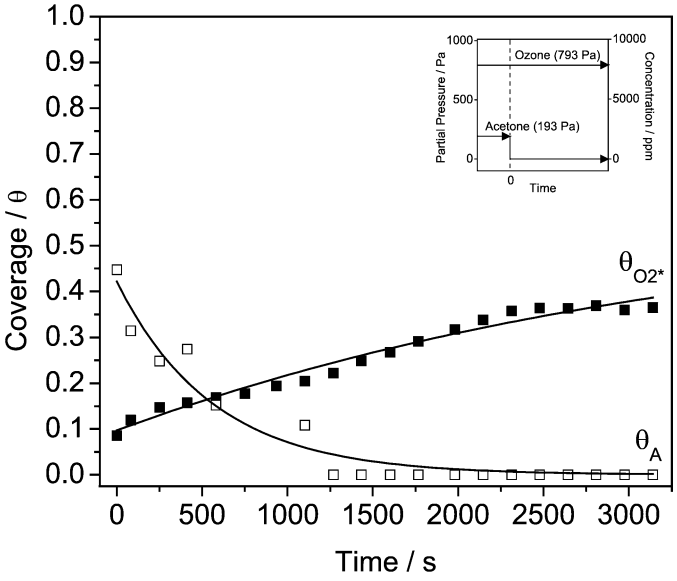

Fig. 13. Transient acetone removal results at 318 K showing coverage values for adsorbed acetone and ozone intermediates as a function of time. The inset shows the inlet partial pressure profiles used for the experiment.

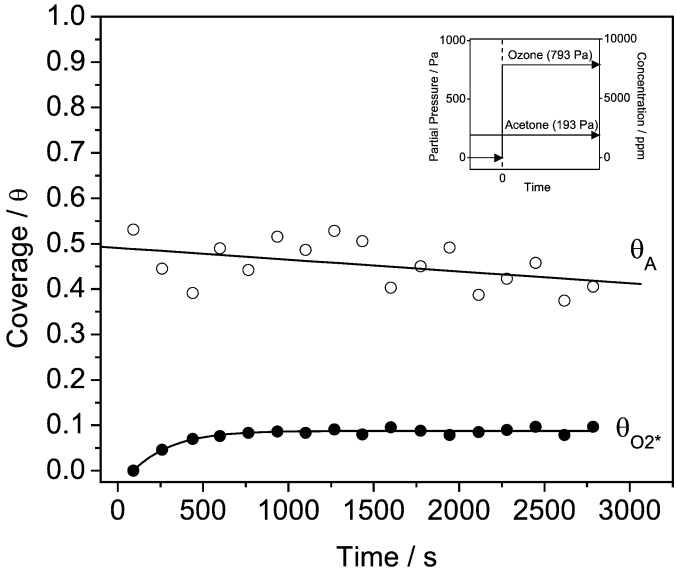

Fig. 14. Transient ozone addition results at 318 K showing coverage values for adsorbed acetone and ozone intermediates as a function of time. The inset shows the inlet partial pressure profiles used for the experiment.

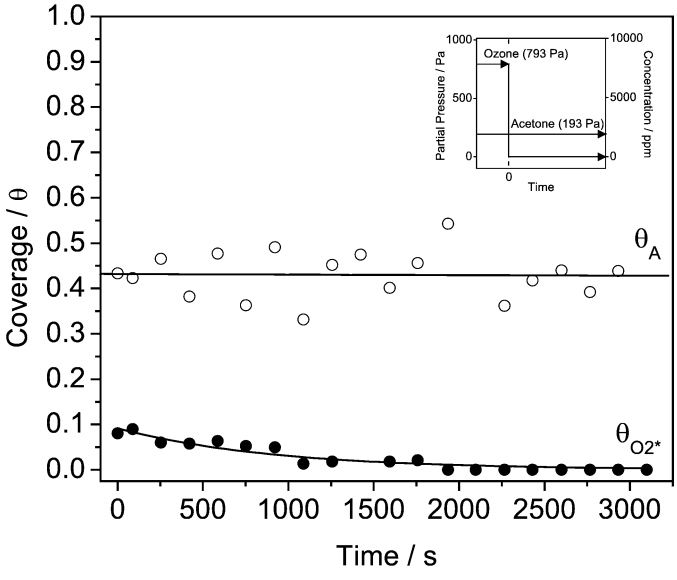

Fig. 15. Transient ozone removal results at 318 K showing coverage values for adsorbed acetone and ozone intermediates as a function of time. The inset shows the inlet partial pressure profiles used for the experiment.

of 0.46 in ∼900 s. Fig. 13 shows the acetone removal results and also includes an inset describing for the experiment. When acetone was removed from the reaction mixture, the coverage associated with the peroxide species gradually increased and took >3000 s to reach a value of 0.38 even though the coverage associated with the acetone intermediate decreased to zero in ∼1250 s. Fig. 14 presents the ozone addition results and the partial pressure profiles for the experiment. When ozone was introduced, the coverage associated with the peroxide species quickly increased to a steady value of 0.09 in ∼800 s, whereas the coverage associated with the acetone intermediate seemed to decrease slightly from an initial value of 0.49 to a final value of 0.42 over the time scale shown (∼3000 s). Finally, Fig. 15 shows the ozone removal results along with the partial pressure profiles for the experiment. When ozone was removed from the gas stream, the coverage associated with the peroxide species gradually decreased until no peroxide was detected at ∼1950 s, whereas the coverage associated with the acetone intermediate remained unchanged at 0.43.

4. Discussion

4.1. Acetone oxidation with ozone

Only a few studies have investigated the kinetics and mechanism of acetone oxidation. One of these studied the oxida-

tion of acetone over a preoxidized Ag(111) surface under ultrahigh vacuum (UHV) conditions using reflection absorption IR [19] and found that at 180 K, acetone adsorbed to form both propane-2,2-diyldioxy and acetone enolate via O-mediated nucleophilic addition and H abstraction. At ∼220 K, the acetone enolate was oxidized rapidly to produce transient metallacyclic intermediates and eventually stable ketenylidene and formate species. Isotopic labeling experiments showed that ketenylidene kept the acetone carbonyl group while the formate was formed from the acetone methyl group and surface O [19]. Another study [20] investigated the kinetics of the photocatalyzed oxidation of acetone (30–170 ppm) in air over a ceramic honeycomb monolith coated with TiO_2. The rate expression for the disappearance of acetone took a Langmuir–Hinshelwood form. A third study [21] investigated the mechanism and kinetics of catalytic partial oxidation of acetone on vanadium pentoxide at 413–453 K. The main partial oxidation products were acetic acid, methanol, and carbon dioxide with minor amounts of formaldehyde and acetaldehyde. The order of the reaction for both acetone and oxygen ranged from zero to one, whereas the activation energy was found to be ∼75 kJ/mol, and the mechanism was consistent with alternating redox steps. The data obtained agreed with the proposed mechanism and the derived kinetic expression except when the concentration of oxygen was varied, and it was concluded that the catalyst reoxidation step was complex [21].

4.2. TPD measurements

Previous oxygen chemisorption measurements on the 10 wt% MnO_x/SiO_2 catalyst used in this study reported the number of reduced surface manganese atoms on the supported catalysts as 98 μmol/g [4]. Dispersion values based on the atomic oxygen chemisorption measurements were compared with dispersion values based on X-ray diffraction (XRD) line-broadening results, and the two techniques were found to yield similar results. Thus it was concluded that oxygen chemisorption measurements give a reasonable estimate of the number of surface manganese atoms. In this work, ozone TPD results gave a saturation peroxide adsorption value of 14 μmol/g. Thus, at maximum peroxide adsorption, only ∼14% of the surface manganese atoms adsorbed a peroxide species. Acetone TPD experiments gave very different results, however. On the 10 wt% MnO_x/SiO_2 catalyst, the saturation amount of acetone intermediate adsorbed on the catalyst surface was 550 μmol/g. Because this value was ∼5.5 times the value obtained for the total number of surface manganese atoms, it can be concluded that most of the adsorbed acetone was located on the silica support. Acetone TPD experiments performed on pure silica resulted in a saturation adsorption value of 790 μmol/g. The BET surface area of the silica and the 10 wt% MnO_x/SiO_2 sample were 320 and 210 m^2/g, respectively. Normalizing the acetone TPD results with respect to surface area gave maximum acetone adsorption values of 2.5 and 2.6 μmol/m^2 for both pure silica and the 10 wt% MnO_x/SiO_2 sample, respectively (Table 1). Therefore, the amount of acetone adsorbed on the pure silica was essentially the same as the amount of acetone adsorbed on the 10 wt% MnO_x/SiO_2 sample based on surface area. This further confirmed that most of the adsorbed acetone for the 10 wt% MnO_x/SiO_2 catalyst was located on the silica support rather than on the surface Mn atoms. Thus, although the coverages reported in this study are based on saturation adsorption, the coverages for the peroxide species are for occupation of the Mn sites, whereas the coverages for the acetone species are for occupation of the silica support.

4.3. Steady-state Raman spectroscopy measurements

Fig. 2 compares Raman experiments done on pure, calcined silica and the 10 wt% MnO_x/SiO_2 catalyst in acetone flow at 298 K, to gain further understanding into the nature of acetone adsorption. Figs. 2a and b show the Raman spectra for the 10 wt% MnO_x/SiO_2 catalyst when acetone was included in the gas mixture at a concentration of 0.2 and 0.4 mol%, respectively. Figs. 2c and d display the Raman spectra for the pure silica when the concentration of acetone was 0.2 and 0.4 mol%, respectively. The feature at 2930 cm^{-1} (Fig. 2) was attributed to the adsorbed acetone intermediate and was assigned to a CH_3 symmetric stretching mode (ν_2, A_1) from data in the literature [22]. The features in Figs. 2c and d located at 798 and 1710 cm^{-1} were assigned to a C–C stretching mode and a C–O stretching mode, respectively. These features observed for the adsorbed acetone intermediate on the pure silica sample were close to the Raman bands reported for liquid phase acetone with bands at 778, 1711, and 2924 cm^{-1} for C–C, C–O, and CH_3 stretching modes, respectively [23]. The intensities for these features were reported to be strong for the C–C stretching mode, intermediate for the C–O stretching mode, and strong for the CH_3 stretching mode [23]. However, for the Raman experiments conducted, the feature (2930 cm^{-1}) attributed to the CH_3 stretching mode was significantly stronger in intensity than the feature (1710 cm^{-1}) attributed to the C–O stretching mode. This gives evidence that the molecularly adsorbed acetone intermediate bonds to the catalyst surface via the oxygen atom. Further Raman experiments on the pure silica sample in acetone flow showed that heating to only 353 K resulted in a large decrease in peak intensities, whereas further heating to just 393 K resulted in the complete disappearance of the bands. These experiments confirm that the acetone was physisorbed on the sample surface, for signals from gas phase acetone would not have decreased so drastically with temperature. Also, these Raman results indicate that acetone adsorbed molecularly on the silica surface with retention of CH_3, C–O, and C–C stretching modes.

Another result from the spectra in Fig. 2 is that the peak intensities and areas for the band located at 2930 cm^{-1} were much greater (∼10×) for the pure silica sample compared with the 10 wt% MnO_x/SiO_2 sample. Also, there were no observable bands located at 798 and 1710 cm^{-1} for the 10 wt% MnO_x/SiO_2 sample. An initial conclusion resulting from these spectra would be that more acetone adsorbs on the pure silica than on the 10 wt% MnO_x/SiO_2 catalyst. However, it must be considered that the surface area of the SiO_2 support (320 m^2/g) was larger than that of the catalyst (210 m^2/g) (Table 1) and

that the white color of the pure silica sample resulted in clearer and more intense Raman signals compared to the dark (black) 10 wt% MnO_x/SiO_2 sample. Therefore, the acetone TPD results should be reliable, and the conclusion that similar amounts of acetone, based on surface area, are adsorbed on both samples under the same conditions is firm. It was also observed that the same acetone coverage was obtained in approaching a temperature from higher and lower values, indicating that the acetone adsorption was equilibrated.

Also, it is important to note that including ozone in the mixture gas for the Raman experiments on pure silica had no effect on the resulting spectra. Ozone was not seen to adsorb on the pure silica sample (Table 1), and ozone did not affect the peak intensity or area for the bands associated with the adsorbed acetone intermediate when both acetone and ozone were included in the reaction mixture.

Figs. 3 and 4 display the spectra for the steady-state, in situ Raman spectroscopy experiments conducted on the 10 wt% MnO_x/SiO_2 catalyst at 318 K using the same varying partial pressure conditions used in the steady-state kinetic experiments. Fig. 3 shows the spectra when the acetone partial pressure was varied (93–394 Pa), and Fig. 4 shows the spectra when the ozone partial pressure was varied (274–1097 Pa). As the partial pressure of acetone was increased (Fig. 3), the peak intensity associated with the adsorbed acetone intermediate (2930 cm^{-1}) increased. However, the increased partial pressure of acetone had little effect on the peak intensity associated with the adsorbed peroxide species (890 cm^{-1}). As the partial pressure of ozone was increased (Fig. 4), the peak intensity associated with the adsorbed acetone intermediate (2930 cm^{-1}) decreased slightly, whereas the peak intensity associated with the adsorbed peroxide species slightly increased.

Surface coverages were calculated for the two adsorbed intermediates using the Raman spectra shown in Figs. 3 and 4. Fig. 5 displays the coverages associated with acetone (θ_A) and ozone (θ_{O_2*}) when the partial pressure of acetone was varied, and Fig. 6 shows the coverages when the partial pressure of ozone was varied. Fig. 5 shows that the coverage of the acetone intermediate increased with increasing partial pressure of acetone, whereas the coverage of the peroxide species was essentially unchanged. Fig. 5 also shows the increase in coverage attributed to the acetone intermediate when the initial partial pressure of acetone was increased and ozone was absent from the reacting mixture. Interestingly, the coverage associated with the adsorbed acetone intermediate was similar regardless of whether ozone was included in the reacting mixture. This is consistent with its adsorption being equilibrated. Fig. 6 shows that the coverage of the acetone species decreased very slightly with increasing partial pressure of ozone, whereas the coverage of the peroxide intermediate increased also only slightly. Fig. 6 also shows the increase in coverage for the peroxide species when the initial partial pressure of ozone was increased and acetone was not included in the reacting mixture. Unlike the effect seen in the coverage of the acetone intermediate, the coverage for the adsorbed peroxide species was drastically reduced when acetone was included in the reaction mixture. All of these observations are consistent with the adsorbed acetone and peroxide species being reaction intermediates. But, as will be seen, this is not the case.

4.4. Steady-state kinetic analysis

A previous acetone/ozone reactivity study [4] performed on the 10 wt% MnO_x/SiO_2 catalyst found that the reaction was homogeneous at high temperatures ($T > 475$ K) but catalytic at low temperatures ($T < 400$ K). In this work, a detailed kinetic analysis was conducted in the lower temperature regime. The measurements were conducted in the apparatus shown in Fig. 1, and only data at low conversions (<10%) were used in the analysis. The resulting kinetic data were used to determine the kinetic parameters for both reactants using two different types of rate expressions, a power-rate law and a Langmuir–Hinshelwood expression.

The power-rate law model had four unknown parameters (A, E_a, α, β) and took the form

$$\text{TOF} = A\exp\left(\frac{-E_a}{RT}\right)C_A^{\alpha}C_{O_3}^{\beta}, \tag{1}$$

where TOF is the turnover frequency, A is the frequency factor, E_a is the apparent activation energy, R is the gas constant, T is the temperature (K), C_A is the concentration of acetone (mol/m^3), C_{O_3} is the concentration of ozone (mol/m^3), and α and β are the orders with respect to acetone and ozone concentration, respectively.

To determine the rate expression for acetone conversion, the entire dataset, consisting of the concentrations of both reactants, acetone TOFs, and all temperatures, was simultaneously fit to an expression of the foregoing form using nonlinear least squares regression analysis [Figs. 7a–10a]. The rate of acetone conversion using all of the data was found to be

$$\text{Acetone TOF} = 0.0797\exp\left(\frac{-7.05\ \text{kJ/mol}}{RT}\right)C_A^{0.194}C_{O_3}^{0.634}. \tag{2}$$

The fitting analysis resulted in a R^2 degree of fit and variance values of 0.834 and 5.16×10^{-7}, respectively. The data for each temperature were then regressed using a common slope based on the foregoing overall fit. When acetone TOF was varied with respect to partial pressure of acetone, the slope ($\alpha = 0.194$) was held constant, and when acetone TOF was varied with respect to partial pressure of ozone, the slope ($\beta = 0.634$) was held constant. The lines in Figs. 7a and 8a show the individual, regressed fits at each temperature for the power rate law expressions for acetone TOF against the actual kinetic data.

The rate expression for ozone conversion was found in the same manner as the rate expression for acetone conversion. The rate of ozone conversion using all the data was found to be

$$\text{Ozone TOF} = 2.04\exp\left(\frac{-10.0\ \text{kJ/mol}}{RT}\right)C_A^{-0.133}C_{O_3}^{1.71}. \tag{3}$$

The fitting analysis resulted in a R^2 degree of fit and variance values of 0.823 and 5.73×10^{-5}, respectively. Figs. 9a and 10a display the individual regressed fits at each temperature for the power rate law expressions for ozone TOF against the actual

Table 2
Non-linear least squares regression results for the kinetic data utilizing the power rate law expressions

T (K)	A	E_a (kJ/mol)	α	β	R^2	Variance
Power rate law expression: Acetone TOF $= A\exp(\frac{-E_a}{RT})C_A^{\alpha}C_{O_3}^{\beta}$						
318, 333, 353, 373	0.0797	7.05	0.194	0.634	0.834	5.16×10^{-7}
318 (vary acetone)	0.0700	7.37	0.194	0.482	0.789	2.10×10^{-7}
333 (vary acetone)	0.0799	7.03	0.194	0.595	0.805	4.75×10^{-7}
353 (vary acetone)	0.0759	7.18	0.194	0.539	0.827	3.88×10^{-7}
373 (vary acetone)	0.0846	6.86	0.194	0.750	0.799	8.04×10^{-7}
318 (vary ozone)	0.0843	6.89	0.266	0.634	0.774	2.25×10^{-7}
333 (vary ozone)	0.0968	6.48	0.331	0.634	0.856	3.32×10^{-7}
353 (vary ozone)	0.0807	7.01	0.195	0.634	0.810	4.24×10^{-7}
373 (vary ozone)	0.0690	7.61	0.091	0.634	0.771	7.60×10^{-7}
Power rate law expression: Ozone TOF $= A\exp(\frac{-E_a}{RT})C_A^{\alpha}C_{O_3}^{\beta}$						
318, 333, 353, 373	2.04	10.0	−0.133	1.71	0.823	5.73×10^{-5}
318 (vary acetone)	1.52	10.8	−0.133	1.27	0.812	1.70×10^{-5}
333 (vary acetone)	1.71	10.5	−0.133	1.37	0.745	5.85×10^{-5}
353 (vary acetone)	2.02	10.1	−0.133	1.68	0.859	4.31×10^{-5}
373 (vary acetone)	2.36	9.57	−0.133	1.98	0.769	1.23×10^{-4}
318 (vary ozone)	1.98	10.1	−0.133	1.71	0.761	2.16×10^{-5}
333 (vary ozone)	1.87	10.3	−0.209	1.71	0.733	6.11×10^{-5}
353 (vary ozone)	1.73	10.5	−0.264	1.71	0.888	3.69×10^{-5}
373 (vary ozone)	2.34	9.53	−0.005	1.71	0.776	1.19×10^{-4}

kinetic data. The entire fitting results and statistical parameters for the power rate law rate expressions are given in Table 2.

The proposed power rate law expressions show that the calculated activation energies for acetone and ozone conversion are 7.1 and 10.0 kJ/mol, respectively. These values are close to those (7.3 and 13.8 kJ/mol, respectively) found in a previous reactivity study done on the same 10 wt% MnO_2/SiO_2 catalyst [4]. The similarity in activation energies for these two studies confirms that in this temperature range, the reaction takes place mainly on the catalyst surface.

Langmuir–Hinshelwood kinetic rate expressions were also obtained from a proposed mechanism detailing the acetone oxidation reaction with ozone over the catalyst. Even though other steps may be involved in the actual mechanism, many of the proposed steps have been verified and are discussed here. The proposed mechanism is as follows:

$$O_3 + {}^* \rightarrow O_2 + O^*, \tag{4}$$

$$O_3 + O^* \rightarrow O_2 + O_2{}^*, \tag{5}$$

$$O_2{}^* \rightarrow O_2 + {}^*, \tag{6}$$

$$A + \square \rightleftharpoons A\square, \tag{7}$$

$$A\square + {}^* \rightleftharpoons A^* + \square, \tag{8}$$

$$A^* + nO^* \rightarrow \text{products}, \tag{9}$$

where * represents a surface manganese site, □ represents a surface silica site, and A represents acetone (CH_3COCH_3).

The first three steps of the proposed mechanism are well understood for ozone decomposition on manganese oxide based on kinetic, spectroscopic, ab initio calculations, and isotopic substitution [14,15]. Even though these steps have been verified, they are briefly explained here. Raman spectroscopy was used to identify a band at 884 cm^{-1} that appeared during the decomposition reaction of ozone, and isotopic substitution experiments allowed the identification of the 884 cm^{-1} peak as belonging to a surface peroxide species ($O_2{}^{2-}$). This assignment was confirmed through ab initio calculations done on a model $Mn(OH)_4(O_2)$ complex that resulted in a vibrational frequency of 899 cm^{-1}, which is in excellent agreement with the frequency observed in the spectroscopic experiments. Isotopic substitution experiments demonstrated that the peroxide species was formed through atomic oxygen species, thus rationalizing the first two steps [Eqs. (4) and (5)] of the proposed mechanism. The third step [Eq. (6)] was verified by removing ozone from the reaction gas mixture and observing the gradual decay in the peroxide signal (884 cm^{-1}) over time. This final step for ozone decomposition, where the peroxide species decomposes to form gas phase molecular oxygen, is a slow step and was shown to be irreversible, because reactions with oxygen alone did not form the adsorbed peroxide species at any condition [14].

It is known from the Raman experiments that even during the reaction with acetone, an adsorbed peroxide species is observed on the catalyst surface at 890 cm^{-1}. It is reasonable that this adsorbed peroxide species is formed in the same way as in the ozone decomposition reaction. Also, in the temperature range used for the kinetic analysis, the TOFs for the ozone were about 10× larger than the TOFs for the acetone reaction. Therefore, a reasonable, overall stoichiometry for the reaction between acetone and ozone is as follows:

$$CH_3COCH_3 + 8O_3 \rightarrow 3CO_2 + 3H_2O + 8O_2, \tag{10}$$

where each ozone molecule contributes a single oxygen equivalent to the reaction and produces an oxygen molecule. From the rate of ozone usage, it can be concluded that the decomposition of ozone takes place simultaneously with the oxidation reaction. Validation of the fourth step [Eq. (7)] comes through the acetone TPD results, which demonstrated that nearly all of the adsorbed acetone was located on the silica support. Raman spectroscopy experiments conducted on a pure silica sample in acetone flow (Fig. 2) confirmed that the silica had a strong affinity for acetone at low temperatures (<373 K). The Raman studies identified an adsorbed acetone intermediate with a CH_3 symmetric stretching mode at 2930 cm^{-1}, a C–C stretching mode at 798 cm^{-1}, and a C–O stretching mode at 1710 cm^{-1}, which gave evidence that the acetone was adsorbed molecularly because the C–H and C–O bonds were intact.

Most likely the silica support acted as a reservoir for the adsorbed acetone intermediates until reaction, when the adsorbed acetone migrated to an active Mn center [Eq. (8)] and then reacted with an atomically adsorbed oxygen species to form products as is shown in the last step [Eq. (9)] of the proposed mechanism. There is evidence that the adsorbed acetone intermediate reacts with an adsorbed atomic oxygen species rather than with the adsorbed peroxide species. As discussed later in detail, transient kinetic experiments prove that the adsorbed peroxide species is a spectator in the acetone oxidation reaction, and thus an adsorbed atomic oxygen species is the likely re-

active intermediate. These atomic oxygen species are highly reactive, quickly converting to peroxide species in the absence of acetone, and are not observed. Raman experiments on the 10 wt% MnO_x/SiO_2 catalyst showed a dramatic decrease in the concentration of the peroxide intermediate with the characteristic band at 890 cm^{-1} when acetone was added to the reaction mixture. Initially, it might appear that the adsorbed peroxide species decreased because acetone competes for active catalyst sites. However, a more reasonable explanation is that the atomic oxygen species produced in the first step of the proposed mechanism [Eq. (4)] were immediately used in the acetone oxidation reaction [Eq. (9)], and thus less of these species were available for peroxide formation [Eq. (5)]. This then led to the observed decrease in peroxide coverage when acetone was included in the reaction mixture, as shown in Fig. 6.

Raman spectroscopy experiments also aided in determining that Eqs. (7) and (8) were equilibrated based on the observation of rapid decay and recovery of the adsorbed acetone coverage when acetone was removed from or added to the gas mixture. Moreover, the acetone coverage for a given set of conditions was always constant regardless of whether approaching from a lower or a higher temperature, further confirming the equilibrium of acetone adsorption. Acetone TPD experiments done on the 10 wt% MnO_x/SiO_2 catalyst confirmed the reversibility of Eq. (7) because gas phase acetone was the only desorption product observed.

The last step consists of a dual-site reaction between an adsorbed acetone intermediate and an adsorbed atomic oxygen species, eventually resulting in complete oxidation. This step can be considered a slow step for the acetone reaction. It is followed by a series of fast steps (not shown) involving reactive acetone fragments and active oxygen species from ozone that produce the CO_2 observed as the reaction product.

Based on the proposed mechanism, rate expressions of the Langmuir–Hinshelwood type were developed for the rate of disappearance of both acetone and ozone. The adsorbed species on the manganese oxide were assumed to be the peroxide species observed in the Raman experiments and an acetone species. Eq. (9) was used to develop the rate of acetone disappearance, giving the expression

$$-r'_A = r_6 = k_6(A^*)(O^*)^n. \tag{11}$$

The concentration of the adsorbed peroxide species was obtained by assuming $r_1 = r_3$,

$$(O_2{}^*) = \frac{k_1}{k_3}(O_3)(^*), \tag{12}$$

where k_1 is the rate constant for the first step [Eq. (4)], k_3 is the rate constant for the third step [Eq. (6)], and $(^*)$ is the concentration of vacant catalyst sites. The concentration of the adsorbed acetone species was obtained assuming the fourth and fifth steps [Eqs. (7) and (8)] are in equilibrium,

$$(A^*) = K_4K_5(A)(^*), \tag{13}$$

where K_4 and K_5 are the respective equilibrium adsorption constants. Performing a total manganese site balance and assuming that the concentration of adsorbed atomic oxygen, (O^*), is very small compared with the other adsorbed intermediates, the concentration of vacant sites, $(^*)$, can be determined to be

$$(^*) = \frac{(L)}{1 + \frac{k_1}{k_3}(O_3) + K_4K_5(A)} = \frac{(L)}{1 + k''(O_3) + K(A)}, \tag{14}$$

where (L) is the total concentration of active catalyst sites. The assumption that the concentration of adsorbed atomic oxygen is much less than that of the other adsorbates is justified considering that Raman spectroscopy did not identify a feature attributed to that intermediate. Therefore, the Langmuir–Hinshelwood rate expressions take the form

$$-r'_A = \frac{k'(A)(O_3)^n}{[1 + k''(O_3) + K(A)]^{1+n}} \tag{15}$$

and

$$-r'_{O_3} = \frac{k'''(O_3)^2}{[1 + k''(O_3) + K(A)]^2}. \tag{16}$$

To simplify the rate of acetone disappearance, the variable n was set equal to 1, assuming that one adsorbed acetone intermediate reacts with one adsorbed oxygen species in the last step [Eq. (9)] of the proposed mechanism. This assumption is reasonable and results in a squared term in the denominator of the expressions, which is typical for such a dual-site mechanism. Both of the Langmuir–Hinshelwood rate expressions derived for the disappearance of acetone and ozone have three unknown parameters. Unlike the power rate law rate expressions, these Langmuir–Hinshelwood kinetic expressions do not include a temperature term. Therefore, to determine the rate of acetone disappearance, the dataset specific to one temperature, consisting of the concentrations of both reactants and acetone TOFs, was simultaneously fit to the foregoing expression for $-r'_A$ using nonlinear least squares regression analysis. This fitting procedure was then repeated for each reaction temperature (318, 333, 353, and 373 K). Once the kinetic parameters (k', k'', and K) were calculated for each temperature, they were regressed using the Arrhenius (k' and k'') or van't Hoff (K) equations to determine expressions for each kinetic parameter as a function of temperature. These expressions were then substituted into the Langmuir–Hinshelwood rate expression for acetone to determine an overall fit as a function of temperature. An identical procedure was carried out for ozone to give the following expressions:

$$-r'_A = \frac{28.0\exp(\frac{-1350}{T})(A)(O_3)}{\left[1 + 0.413\exp(\frac{532}{T})(O_3) + 133\exp(\frac{-818}{T})(A)\right]^2} \tag{17}$$

and

$$-r'_{O_3} = \frac{0.730\exp(\frac{-262}{T})(O_3)^2}{\left[1 + 7.66\times10^{-5}\exp(\frac{3320}{T})(O_3) + 7.84\exp(\frac{-456}{T})(A)\right]^2}. \tag{18}$$

Table 3 presents the fitting results for the derived Langmuir–Hinshelwood rate expression based on the proposed mechanism, including statistical parameters. Figs. 7b–10b show the fits with respect to the actual kinetic data.

Table 3
Non-linear least squares regression results for the kinetic data utilizing the Langmuir–Hinshelwood expressions

T (K)	k' (s^{-1} $(m^3/mol)^2$)	k'' (m^3/mol)	K (m^3/mol)	R^2	Variance
		Langmuir–Hinshelwood expression: Acetone TOF $= \frac{k'(A)(O_3)}{[1+k''(O_3)+K(A)]^2}$			
318	0.454	2.44	11.7	0.829	1.70×10^{-7}
333	0.396	1.59	9.07	0.851	3.64×10^{-7}
353	0.706	2.31	13.6	0.842	3.55×10^{-7}
373	0.744	1.61	15.5	0.720	7.51×10^{-7}
Regression	$28.0\exp(\frac{-11.2\ \text{kJ/mol}}{RT})$	$0.413\exp(\frac{4.43\ \text{kJ/mol}}{RT})$	$133\exp(\frac{-6.80\ \text{kJ/mol}}{RT})$		
T (K)	k''' (s^{-1} $(m^3/mol)^2$)	k'' (m^3/mol)	K (m^3/mol)	R^2	Variance
		Langmuir–Hinshelwood expression: Ozone TOF $= \frac{k'''(O_3)^2}{[1+k''(O_3)+K(A)]^2}$			
318	0.320	2.40	2.13	0.820	1.32×10^{-6}
333	0.332	1.84	1.58	0.728	5.09×10^{-6}
353	0.289	0.864	2.40	0.892	2.88×10^{-6}
373	0.156	−0.0446	0.218	0.786	9.32×10^{-6}
Regression	$0.730\exp(\frac{-2.18\ \text{kJ/mol}}{RT})$	$7.66 \times 10^{-5}\exp(\frac{27.6\ \text{kJ/mol}}{RT})$	$7.84\exp(\frac{-3.79\ \text{kJ/mol}}{RT})$		

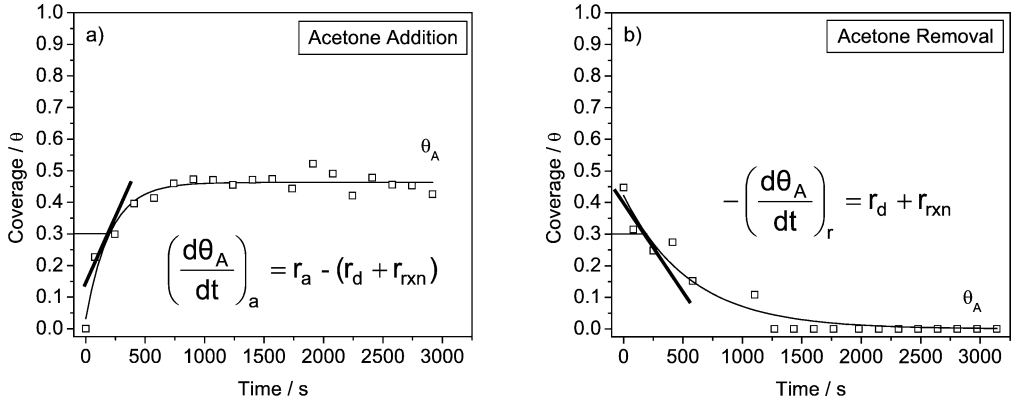

Fig. 16. Transient kinetic analysis example for (a) acetone addition and (b) acetone removal.

Comparing Tables 2 and 3 shows that the fitting statistic values (R^2 and variance) for the power rate law rate expressions and the Langmuir–Hinshelwood rate expressions are quite similar and cannot be used to discriminate between the rate expressions. Even though the variances calculated for the ozone rates are an order of magnitude smaller for the Langmuir–Hinshelwood expression compared with the power rate law, the R^2 degree of fits are comparable. The Langmuir–Hinshelwood expression for the rate of acetone disappearance gives reasonable kinetic parameters and fits, and thus the proposed mechanism does match the data for the acetone reaction. The Langmuir–Hinshelwood expression for the disappearance of ozone also gives reasonable fits, even though one of the optimized parameters (k'' at 373 K; Table 3) is physically not realistic.

4.5. Transient kinetic analysis

Even though it is important to identify the reactive intermediates involved in a catalytic reaction to elucidate a mechanism, it is equally important to recognize that observed adsorbed species do not always play a role in the overall catalytic cycle [24]. Sometimes they can be just spectators on a surface [25]. Therefore, determining an adsorbate's contribution to the overall catalytic reaction requires that both steady-state and transient kinetic analysis be performed and compared [1]. Here the dynamic nature of the adsorbed intermediates involved in the reaction between acetone and ozone over a 10 wt% MnO_2/SiO_2 catalyst is discussed using the Tamaru method.

The transient coverage versus time curves (Figs. 12–15) can be used to obtain adsorption and reaction rates as a function of coverage by differentiation of the data. An example of this method for acetone is shown in Fig. 16. Fig. 16a displays the acetone addition curve at 318 K, which shows the evolution of acetone coverage, θ_A, as a function of time when acetone is added to the reaction mixture already containing ozone. The rate of increased coverage, $(d\theta_A/dt)_a$, is equal to the rate of acetone adsorption, r_a, minus the rate of acetone desorption, r_d, minus the rate of acetone reaction, r_{rxn}, or $(d\theta_A/dt)_a = r_a - (r_d + r_{rxn})$. Fig. 16b displays the acetone removal curve, which shows the decay in acetone coverage, θ_A, as a function of time when acetone is removed from the reaction mixture. The rate of decrease in coverage, $-(d\theta_A/dt)_r$, is equal to the sum of the rates of acetone desorption and reaction, or $-(d\theta_A/dt)_r = r_d + r_{rxn}$. The rates for acetone addition and removal were obtained by differentiating both curves with respect to time at the same coverage to obtain the slope (i.e., rate). Once

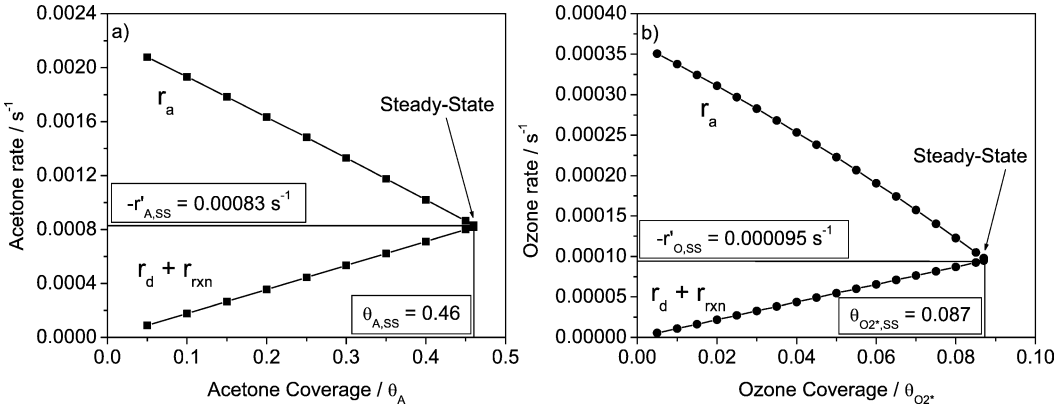

Fig. 17. Transient kinetic analysis results to determine steady-state coverages and rates for (a) acetone and (b) ozone.

the rate of acetone addition, $(d\theta_A/dt)_a$, and rate of acetone removal, $-(d\theta_A/dt)_r$, are obtained, the rate of acetone adsorption can be calculated by the expression $r_a = (d\theta_A/dt)_a - (d\theta_A/dt)_r$ (at the same coverage). The same procedure was followed to determine the rate of ozone adsorption using the ozone addition and removal curves.

Fig. 17 displays the results of the transient analysis with the rate of acetone adsorption plotted with the rate of acetone removal [Fig. 17a] and the rate of ozone adsorption plotted with the rate of ozone removal [Fig. 17b]. Figs. 17a and b show that the rates of adsorption for both acetone and ozone adsorption decreased with increasing coverage, whereas the rates of removal increased with increasing coverage. These dependencies were expected, because the rate of adsorption is proportional to the number of empty sites and the rate of desorption is proportional to the number of occupied sites. At steady state, the rate of adsorption is equal to the rate of removal, so steady-state rate and coverage values can be obtained by the intersection of the two curves. Fig. 17a shows that the steady-state acetone rate was 0.00083 s^{-1} and the steady-state coverage for the adsorbed acetone intermediate was 0.46. Fig. 17b shows that the steady-state ozone rate was 0.000095 s^{-1} and the steady-state coverage for the adsorbed peroxide species was 0.087. Recall that the conditions for the addition and removal experiments used initial partial pressures for acetone and ozone of 193 and 793 Pa (1900 and 7800 ppm), respectively, at a temperature of 318 K. Referring to Figs. 7–10, which display steady-state rate as a function of reactant partial pressure, it can be seen that the steady-state values were 0.0015 s^{-1} and 0.0086 s^{-1} for the overall rates of acetone and ozone reaction, respectively, at the conditions used in the transient experiments. Likewise, referring to Figs. 5 and 6, which display steady-state coverage as a function of varying reactant partial pressure, the steady-state coverage values were 0.36 and 0.081 for the adsorbed acetone and ozone intermediates, respectively, at the conditions used in the transient experiments.

Table 4 compares the steady-state rate and coverage results with the rates and coverages obtained from the transient experiments. As shown, the coverages obtained by the two separate techniques are in good agreement. There is greater error when comparing the coverages obtained by the two techniques for the adsorbed acetone intermediate than for the adsorbed ozone intermediate. This error is due to the small peak intensity and area attributed to the adsorbed acetone intermediate, which resulted in greater error during peak integration. When comparing the rates obtained by the two separate techniques, however, only the acetone results are in reasonable agreement. It is known from experiments that the rates of ozone reaction are ∼10 times the rates of acetone reaction. For the transient results, however, the rate of ozone reaction obtained by monitoring the adsorbed peroxide species is significantly less than the rate of acetone reaction obtained from monitoring the adsorbed acetone intermediate. Thus, it can be concluded that the adsorbed acetone intermediate does contribute to the overall acetone oxidation reaction as described by the reaction mechanism, whereas the adsorbed peroxide species does not contribute to the oxidation reaction. Based on this result, the main reactive species are indicated to be adsorbed atomic oxygen species, as proposed in the mechanism.

Table 4
Steady-state and transient rate and coverage comparison

	Steady-state results	Transient results
Acetone coverage, θ_A	0.36	0.46
Peroxide coverage, θ_{O_2*}	0.081	0.087
$-r'_{A,SS}$ (s^{-1})	0.0015	0.00083
$-r'_{O,SS}$ (s^{-1})	0.0086	0.000095

5. Conclusions

The steady-state and transient kinetics of the oxidation of acetone using ozone over a silica-supported manganese oxide catalyst was studied at 318–373 K. Raman spectroscopy experiments identified an adsorbed acetone species at 2930 cm^{-1} on the silica support and an adsorbed peroxide species due to ozone at 890 cm^{-1} on the manganese oxide. The steady-state kinetics for the acetone and ozone reactions were found to be reasonably described by both a power rate law model and a Langmuir–Hinshelwood model. Transient experiments, conducted for both acetone and ozone, were used to separately measure the rate of reactant adsorption and the rate of reactant removal (desorption plus reaction) to and from the catalyst surface. By setting the rate of adsorption equal to the rate of

removal, steady-state rates for both acetone and ozone reaction, as well as coverages for both the acetone and peroxide intermediates, were calculated. The coverages obtained through the transient experiments compared favorably to those obtained from in situ Raman spectroscopy measurements under steady-state conditions. However, only the steady-state rate of acetone reaction obtained through the transient experiments compared favorably to the results obtained under steady-state conditions. Thus, the adsorbed peroxide species was determined to be a spectator in the acetone oxidation reaction. The mechanism was proposed to involve the reaction between an adsorbed acetone species and an adsorbed atomic oxygen species to initiate the formation of complete oxidation products.

References

[1] S.T. Oyama, W. Li, Top. Catal. 8 (1999) 75.
[2] A. Gervasini, G.C. Vezzoli, V. Ragaini, Catal. Today 29 (1996) 449.
[3] D.V. Maksudov, F.R. Ismagilov, I.Kh. Khairulin, S.R. Khairulin, Z.R. Ismagilov, Eurasian Chem.-Technol. J. 4 (2002) 271.
[4] C. Reed, Y.K. Lee, Y. Xi, S.T. Oyama, J. Phys. Chem., submitted for publication.
[5] Y. Xi, C. Reed, Y.K. Lee, S.T. Oyama, J. Phys. Chem., in press.
[6] X. Su, K.Y. Kung, J. Lahtinen, Y.R. Shen, G.A. Somorjai, J. Mol. Catal. A: Chem. 141 (1999) 9.
[7] P.S. Cremer, G.A. Somorjai, J. Chem. Soc., Faraday Trans. 91 (1995) 3671.
[8] M. Seman, J.N. Kondo, K. Domen, C. Reed, S.T. Oyama, J. Phys. Chem. B 108 (2004) 3231.
[9] S.T. Oyama, R. Radhakrishnan, M. Seman, J.N. Kondo, K. Domen, K. Asakura, J. Phys. Chem. B 107 (2003) 1845.
[10] A.M. Efstathiou, T. Chafik, D. Bianchi, C.O. Bennett, J. Catal. 148 (1994) 224.
[11] I.A. Fisher, A.T. Bell, J. Catal. 184 (1999) 357.
[12] M.A. Brundage, M.W. Balakos, S.S.C. Chuang, J. Catal. 173 (1998) 122.
[13] S. Xie, J.H. Lunsford, Appl. Catal. A. 188 (1999) 137.
[14] W. Li, G.V. Gibbs, S.T. Oyama, J. Am. Chem. Soc. 120 (1998) 9041.
[15] W. Li, S.T. Oyama, J. Am. Chem. Soc. 120 (1998) 9047.
[16] H. Shindo, C. Egawa, T. Onishi, K. Tamaru, J. Chem. Soc., Faraday Trans. I 76 (1980) 280.
[17] R.M. Felder, R.W. Rousseau, Elementary Principles of Chemical Processes, second ed., John Wiley & Sons, New York, 1986, p. 235.
[18] Copyright ©2005, Mordechai Shacham, Michael B. Cutlip and Michael Elly.
[19] W.S. Sim, D.A. King, J. Phys. Chem. 100 (1996) 14794.
[20] M.L. Sauer, D.F. Ollis, J. Catal. 149 (1994) 81.
[21] G.I. Golodets, V.V. Borovik, V.M. Vorotyntsev, Teor. Eksp. Khim. 22 (1986) 252.
[22] G.M. Warnes, Spectrochim. Acta 49A (1993) 45.
[23] F.F. Cleveland, M.J. Murray, J.R. Coley, V.I. Komarewsky, J. Phys. Chem. 10 (1942) 18.
[24] K. Tamaru, Dynamic Heterogeneous Catalysis, Academic Press, London, 1978.
[25] W. Zhang, S.T. Oyama, J. Phys. Chem. 100 (1996) 10759.